CHAPTER-6

Realization and Evaluation of the Experimental S-Band MILO

6.1. Introduction

The major components of S-band MILO are the cathode, choke vanes, SWS vanes, Extractor vane, Beam dump, and Stubs. The dimensions of the aforesaid components have been obtained from analytical equations and further these dimensions are optimized for getting maximum RF power at the output and higher efficiency so that length and weight of the MILO is reduced significantly. Later the piece parts have been fabricated in aluminum material and carried out cold test measurements for getting dispersion characteristics for fundamental mode and it is compared with simulated results. In the previous chapter 5, the RF characteristic parameter ─ dispersion characteristics has been experimentally measured, from which pi-mode frequency of RF interaction structure has been inferred and found as per our design values.

In the present chapter, the piece parts and assembly drawings are made as per the design using solid works modelling software and all the piece parts of S-band MILO are fabricated of stainless steel (SST) material, except window made with perspex material, by using high precision lathe and milling machine at MTRDC, Bangalore. The Vlasov antenna has been designed and fabricated for the testing MILO in laboratory condition. All the parts of MILO are integrated with Marx generator at MTRDC and tested for RF power output and at the oscillator frequency using suitable mode transducer in the TE_{11} mode so that major lobe carries maximum power.

In this chapter, the development, realization and experimental evaluation of S-band MILO are described. The rest of the chapter is organized as follows: Design and simulation of MITL for understanding the concept of self-magnetic insulation is described in Section 6.2. The diagnostic set-up for MILO, including pulsed power and RF power diagnostics are explained in Section 6.3. The design and simulation of Vlasov Antenna and window is described in section 6.4 and the development of S-

band MILO is presented in Section 6.5. Testing and characterization of S-Band MILO is discussed in section 6.6 and the conclusion is drawn in Section 6.7.

6.2. Design and Simulation of MITL for Self-Magnetic Insulation Concept

The MITL has been used for studying the phenomena of self-magnetic field generation for proving the concept of self magnetic insulation between the cathode - anode because MILO works based on the concept of MITL. The self-generation of magnetic field, in a MILO is achieved by current flowing through the outer conductor. The self-magnetic field is generated in response to the relativistic electron flow itself rather than imposed by external magnetic coils, like in the case of the relativistic magnetron, relativistic BWO, etc. The schematic representation of magnetic insulation is shown in Fig. 6.1. When $I < I_{critical,}$ all the electrons reach from the cathode to anode because there is no magnetic insulation is established between cathode and anode. The magnetic insulation is established between cathode and anode when $I > I_{critical}$ and all the electrons are confined between the cathode and anode.

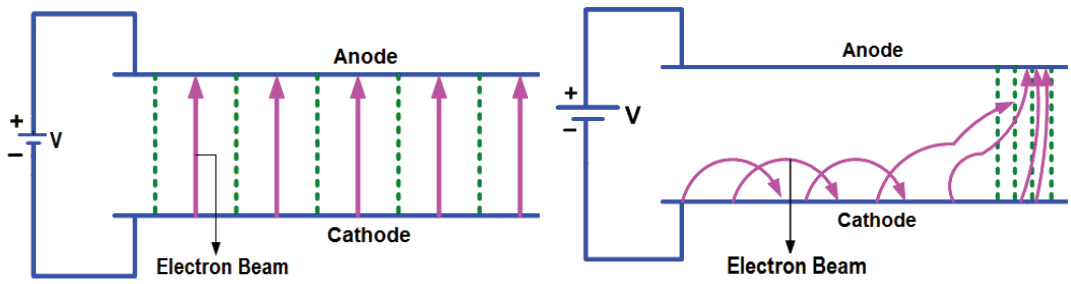

Fig.6.1: Schematic representation of magnetic insulation (*a*) No Magnetic Insulation ($I < I_{critical}$) (*b*) Self-Magnetic Insulation ($I > I_{critical}$) [Bluhm, (2006)] .

This eliminates the need to synchronize the applied beam voltage to the magnetic field, as the insulating magnetic field and accelerating voltage are produced by the same source [Ron *et al*. (1973)], [Smith *et al*. (1977)], [Creedon (1977)], [Capua

(1983)], [Mendel *et al*.(1983)], [Lawconnell and Neri (1990)]. This is the basic concept for producing very high-power microwave pulses in MILO [Bluhm, (2006)]. The self-magnetic insulation study was carried out for a pulse power system operating above the pulse voltage of 500kV and 30 kA beam current. However in this chapter, the design, development and experimental validation of the Magnetically Insulated Transmission Line (MITL) using 200J pulsed power system operating with a single shot having pulse width of 50 to 80 ns for beam voltage of 200kV - 300 kV and current of 8 - 14 kA of current.

6.2.1. Analytical Design of MITL

The preliminary design was carried out based on analytical approach given by [Ron *et al*. (1973)], [Smith *et al*. (1977)], [Creedon (1977)], [DiCapua (1983)], [Mendel *et al*. (1983)], [Lawconnell and Neri (1990)], for obtaining the dimensional details of a MITL.

The current drawing from the geometry I_o should satisfy the following condition for magnetic insulation to occur is given by [smith *et al*. (1977)]:

$$I_o > I_{\min} \quad , \tag{6.1}$$

and $I_{\min} < I_c, I_p$.

Critical current I_c is given by [smith *et al*. (1977)]:

$$I_c = \frac{V_o}{Z_0}\left[\frac{\gamma_o + 1}{\gamma_o - 1}\right] \quad , \tag{6.2}$$

The relativistic factor γ_o is defined as [smith *et al*. (1977)]

$$\gamma_o = 1 + \frac{eV_o}{m_o c^2} \ ,$$

where, V_o is the beam voltage and $Z_o = 60g$ is the characteristic impedance of the diode. Here, $g = \ln(r_i / r_c)$, r_i is SWS vane inner radius and r_c is cathode radius

The parapotential current (I_p) or total anode current (I_t) is given by [smith *et al*. (1977)]

$$I_p(kA) = 8.5\, g\, \gamma_o \ln\left(\gamma_o + \sqrt{\gamma_o^2 - 1}\right) \quad . \tag{6.3}$$

The mimimum current ($I_{\min}$) is given by [Jin and Yuan (2007)] as:

$$I_{\min}(kA) = 8.5\, g\, \gamma_l^3 \ln\left(\gamma_l + \sqrt{\gamma_l^2 - 1}\right) \quad , \tag{6.4}$$

where the relativistic factor of MITL (γ_l) can be determined using numarical method

$$\gamma_o = \gamma_l + \left(\sqrt{\gamma_l^2 - 1}\right)^{3/2} \ln\left(\gamma_l + \sqrt{\gamma_l^2 - 1}\right) \quad . \tag{6.5}$$

Current between anode-cathode gap plus between cathode and collector is computed based on Child's law given by [Lawconnell and Neri (1990)] as:

$$I_o = 2.33\times10^{-6} \lim_{x\to\infty} \frac{V_o}{(r_i - r_c)^2} \times 2\pi r_c l_c + 2.33\times10^{-6} \frac{(V_o)^{3/2}}{d^2} \pi r_c^2 . \tag{6.6}$$

6.2.2. Numerical Simulation of the MITL

For the numerical appreciation of the present analysis, a 3D co-axial transmission line geometry as per the analytical design is modeled as per the dimensions (r_c=23mm; r_i=55mm; Length of MITL=600mm; Length of cathode =200 mm) arrived from the aforesaid equations and it is shown in Fig.6.2. The analysis is carried out using 3D electromagnetic simulation code (CST-Particle studio) following the approach reported in [Capua (1983)]. The center conductor is considered as cathode and outer conductor is considered as the anode. The electrons emission is obtained along the entire cylindrical cathode surface area. The simulation is repeated for the operating voltage from 200kV to 250kV and obtained the emission current from 8kA to 12kA.

The simulated electron trajectory plots for 200kV and 250kV are shown in Fig.6.2.

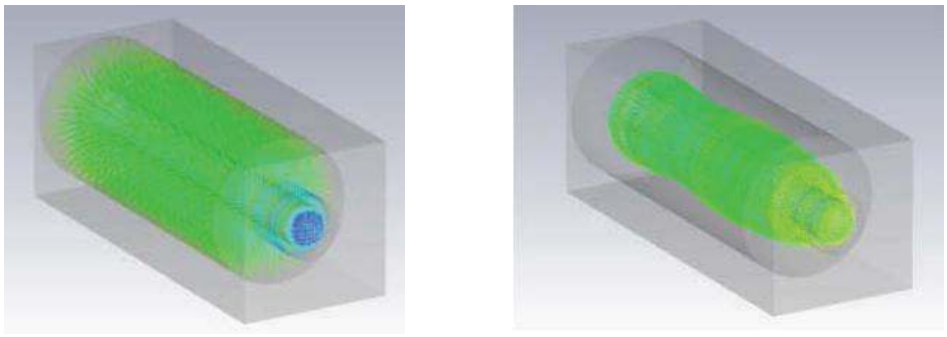

Fig. 6.2: Electron trajectory plots for (*a*) Emission current 8 kA for 200kV and (*b*) Emission current of 12 kA for 250kV.

It is observed from the aforesaid simulation that there is no magnetic insulation occurred between cathode and anode due to less current as shown Fig. 6.2(*a*) and the magnetic insulation has occurred cathode and anode for the emission current of 12 kA at 250kV as shown in Fig.6.2 (*b*).

6.2.3. Electrical Testing of the MITL

The schematic of co-axial magnetically insulated transmission line (MITL) experimental set-up is shown in Fig.6.3. The center conductor is cathode and outer conductor is anode. Cathode of MITL is connected to the center conductor of pulsed power system and outer cylinder is matched to outer cylinder using interface flange. Perspex flange is connected with other end of MITL cylinder to provide vacuum envelope and high voltage isolation.

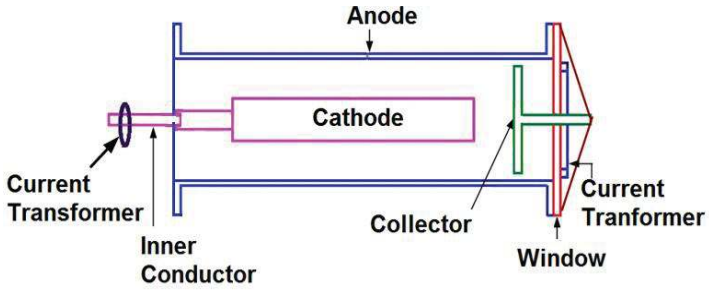

Fig. 6.3 : Schematic of the MITL experimental setup.

The experimental set-up of MITL is interfaced with 200 J pulsed power system as shown in Fig. 6.4. The Rogowski Coil (RC) has been used to measure the total current delivered by the pulsed power system and collector current. The collector has been isolated from anode by perspex flange which is an insulator material. Co-axial ground connection is used to connect collector to outer cylinder for reducing the inductance. Copper Sulphate solution based voltage divider is used to measure the beam voltage. The beam voltage, total anode current and collector current are measured for repeated shots. Fig. 6.5 (*a*) shows the measured pulse voltage of 265kV and measured total current of 13.4kA and collector current of 10.5kA is shown in Fig.6.5 (*b*).

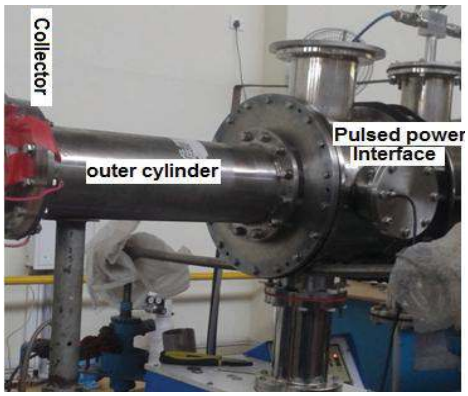

Fig. 6.4 : Experimental set-up of MITL .

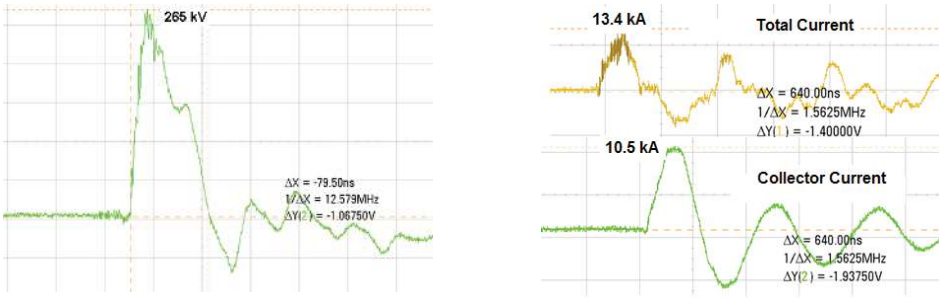

(*a*) (*b*)

Fig. 6.5 : Measured (*a*) voltage pulse (*b*) Current pulse.

It is observed from the above experimental set-up results shown in Fig.6.5 that the collector current of 10.5 kA could be measured only if the self-magnetic insulation

is established and it is confirmed with the analytical design and simulation. The self magnetic insulation occured or not can be confirmed by checking the collector current value. The collector current should be between 70-80% of pulsed current for establishing self- magnetic insulation.

Table 6.1 : Comparison of design and experimental results

Parameters	Results	
	Design	**Experiment**
Pulse volatge	250 kV	265 kV
Pulse current	12 kA	13.4 kA
Total anode current	10 kA	-
Mniimum current required for Magnetic Insulation	11.5 kA	13.4 kA
Collector current	12 kA	10.5 kA

6.3. Diagnostic Set-up for the MILO

Diagnostic requirements of the MILO system is broadly classified into two different categories. i) Pulsed power ii) RF power. Fig .6.6 shows the MILO system along with the diagnostics arrangement.

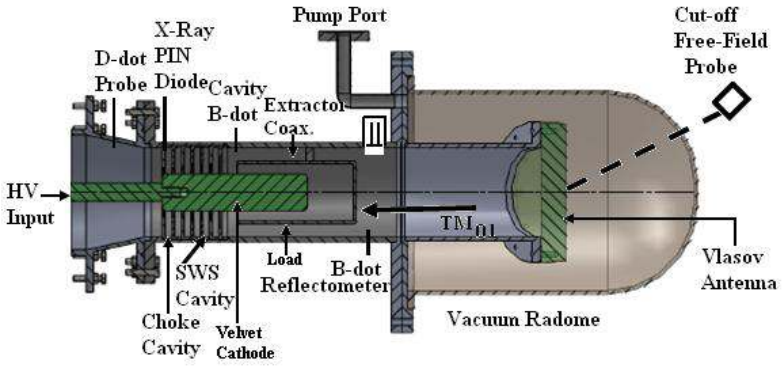

Fig. 6.6 : Diagnostic setup for MILO [Ref: M D Haworth *et al*. (1998)].

6.3.1. Pulsed Power Diagnostics

The voltage measurements are made using voltage dividing circuits. Because of the fast rise times of the diode voltage, the resistive voltage divider was probably not a good choice for the diode voltage diagnostic. Liquid resistor is a better choice for its

main drop resistor due to flexibility in construction and introduces no stray inductance. Secondary resistor also may be liquid resistor or carbon resistor with frequency compensation. The introduction of a low-pass filter will be helping to reduce the ringing due to the stray inductance. The voltage probes were calibrated using commercially available medium voltage probes.

Rogowski coils have been used for decades for non-invasive current measurement when other probe, such as current shunts, current transformers are impracticable. A traditional Rogowski coil comprises a helical wire bent into a toroid through which the current to be measured is passed. Since the pulse rise times are in the nanosecond regime, the traditional Rogowski coil is not usable. When the effect of the winding-shield capacitance is taken into effect, the coil is known as a slow-wave Rogowski coil. A slow wave Rogowski coil operates as a transmission line. The standard model for a transmission line models the distributed series inductance and parallel capacitance as lumped inductors and capacitors per unit length. The ideal place to locate a sensor for the measurement of the diode current would be in the vacuum chamber, situated so that the electron beam current would flow through it. In practice, locating the Rogowski coil in the vacuum chamber would cause many other problems. The insulated wire and winding of the wire could cause virtual leaks in the vacuum system as they outgassed. The coil could be potted in epoxy for preventing outgassing. A slow-wave Rogowski coil requires the outer shield to be at ground potential. Fig.6.7 is a schematic of a Rogowski coil.

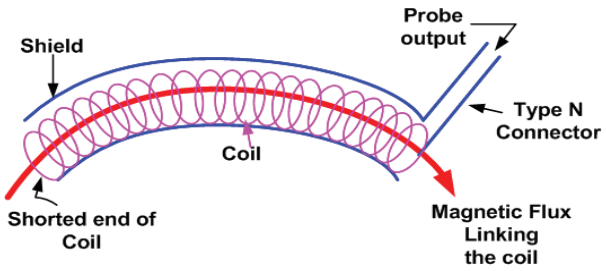

Fig. 6.7 : Schematic of Rogowski coil

The advantages of using a Rogowski coil to measure high frequency currents are:

- Non-saturation, because it is air-cored.
- Good linearity, due to the absence of magnetic materials.
- Simple circuitry and low price.
- Non-intrusive, i.e., the coil does not load the circuit carrying the current to be measured under certain conditions of impedance matching. They draw no power from the main circuit carrying the current to be measured.

The size of the Rogowski coil required remains the same despite the range of current. This is unlike other current transducers which become bulkier as the current magnitude increases.

6.3.2. RF Power Diagnostics

To measure HPM pulses, special probes are needed since the pulses are short and high electromagnetic field strength. The probes must have a short rise time to be able to record the rapid changes of the microwave radiation and a small effective area, otherwise there will be a flashover at the output of the probe. One probe that meets these requirements is the B-dot probe, which basically a small single loop antenna that measures the time derivative of the magnetic field. To lower the inductance and thus giving it a shorter rise time the loop is extended in the axial direction to a cylinder. In order to obtain a differential output, two cylinders are used measuring in opposite directions, when the signals from the two cylinders are added together, the signal is doubled and common mode noise is canceled out. Since there are shot-to-shot variations, measurements of the radiation pattern have to be made at all desired positions at the same time, which requires many probes.

D-dot probes are field coupled sensors which are used to measure impulse voltages; they have attractive features including a non-intrusive installation, simplicity of construction and potentially wide-bandwidth These sensors are used in combination with passive integrators (low-pass filter) providing broad-band capability, but with

limited sensitivity. X-ray PIN diode is used for measuring X-rays coming out of MILO while testing at higher voltages.

Also ,the cut-off free-field probe and microwave detectors have been used to measure the RF power at the output with receiving antenna which is coupled to the detector through appropriate attenuators. The voltage output of the detector is proportional to the input power. The frequency of the microwave signal is found out by carrying out Fast Fourier Transform (FFT)of the signal.

6.4. Design and Simulation of Vlasov Antenna and Window

The MILO device generates RF power at the output in TM_{01} (Transverse Magnetic) mode. The side lobe generation, gain reduction, and inefficient power loading on the antenna aperture, make this mode unsuitable for driving conventional antennas. This gave an idea of using mode converters at the output of MILO to convert from TM_{01} to TE_{11} mode for getting a plane-parallel linearly polarized beam. The mode convertor called Vlasov antenna where the cicular waveguide with certain angle of bevel-cut angle generally lies between 30° and 60° [Benford *et al*.(2007)]. The design and simulation of Vlasov antenna and window are discussed below.

6.4.1. Design of Bevel-Cut Vlasov Antenna and Window

Bevel-cut Vlasov antenna is one of the most known mode converter used with MILO device for laboratory testing as shown in Fig. 6.8. The well-known Vlasov types are the step-cut and the bevel-cut antennas [Ling and Yuan (2004)]. The step-cut, originally suggested by Vlasov, has sharp edges and therefore it may suffer from electrical breakdown when radiating HPM. The bevel-cut, which was later suggested by Nakajima, avoids the sharp points of step cut, and as a result has a more suitable shape for HPM applications. However, a Vlasov antenna with either the bevel or step cut has its maximum radiation shifted by some angle with respect to the axis of the waveguide.

A comparison of the performance of bevel-cut and step-cut Vlasov antennas in HPM is carried out, concluding that the bevel cut has better performance in HPM applications [Ruth *et al*. (1989)]. To test MILO device at laboratory level in TE_{11} mode, bevel-cut Vlasov antenna is designed and simulated with perspex window using CST studio.

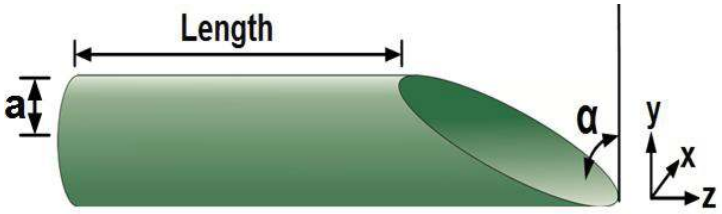

Fig. 6.8 : Schematic of Bevel-cut Vlasov antenna

The cut angle 'α' is shown in Fig. 6.8 and is the single parameter available for optimization, and it has the main effect on the gain and radiation patterns of the antenna. The angle that maximizes the gain of the antenna is given by [Fazaelifar and Fatorehchy (2008)].

$$\alpha = \sin^{-1}[(\rho_{0n}\,\lambda)/(2\pi\,\mathrm{a})] \tag{6.7}$$

where ρ_{0n} is the *n*-th root of the equation $J_0(\rho_{0n}) = 0$, , λ is the wavelength, *a* is the inner radius of the circular waveguide, and J_0 is the Bessel function of the first kind and zeroth order.

For the TM_{01} circular waveguide designed for 3.3 GHz, a = 61.4mm and , λ = 90.1mm. Also, ρ_{0n} =2.405, thus the bevel cut angle is calculated by using equation (6.7)

$$\alpha = \sin^{-1}[(2.405\times 90.1\times 10^{-3})/(2\pi\times 61.4\times 10^{-3})] = 34^\circ \ .$$

The highest gain according to the equation is obtained at a cut angle of 34°.

For this angle, the theoretical peak gain is given by [Benford *et al*. (2016)] :

$$G = \left[6.36\left(\frac{D}{\lambda}\right)^2\right]/\cos\theta \qquad . \tag{6.8}$$

The perspex window is connected at the output of Vlasov bevel-cut antenna for maintaining the vacuum around 10^{-5} Torr inside the MILO as well as transmitting the microwaves to free space without attenuation.

The thickness the perspex window is generally given by :

$$\text{Thickness of window } (T) = \lambda / (2 \times \sqrt{\varepsilon_r}) \quad (6.9)$$

where λ =90.1mm; ε_r =2.6 for perspex material. Using the equation (6.9), the thickness of the perspex window is calculated as 30mm. The theoretical gain calculated using the equation (6.8) is 14.2 dB. The gain value simulated through CST Microwave studio, is 12.8dB, as shown in Fig.6.10.

6.4.2. Simulation of Bevel-Cut Vlasov Antenna and Window

Vlasov antenna with bevel cut angle of 34° and legth of 300mm and window of elliptical shape with 30mm thickness is modeled in CST and simulated in CST studio as shown in Fig.6.9(*a*). Bevel-cut Vlasov antenna and window are defined as perfect electric conductor (PEC) and insulator material in simulation respectively. Open boundary is assigned in x, y and z axis direction .In CST microwave studio. Time domain solver is used in the simulation for solving the the farfiled parameters. Field minitor is defined in farfiled at 3.3 GHz to observe E-field and H-field pattern and realized gain. The Fig. 6.9(*b*) shows the bevel-cut Vlasov antenna gives a maximum computed realized gain of 12.8 dB, with the maximum radiation along the θ = 9° and ϕ = 90° direction. The Half Power Beam width (HPBW) of 35.2° with side lobe level of -15.5dB are obtained from simulation as shown in Fig. 6.10. The bevel-cut antenna operates at 3.3GHz with the VSWR plot as shown in Fig. 6.11 in which VSWR of 1.09 is obtained at 3.3GHz and it is within the acceptable limit of operation.

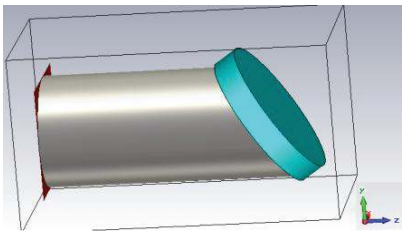

(a)

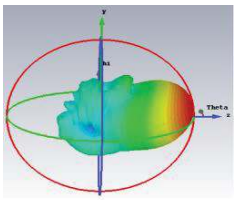

(b)

Fig. 6.9 : (*a*) 3D model of Vlasov antenna with window and (b) Bevel cut 3D gain pattern using CST .

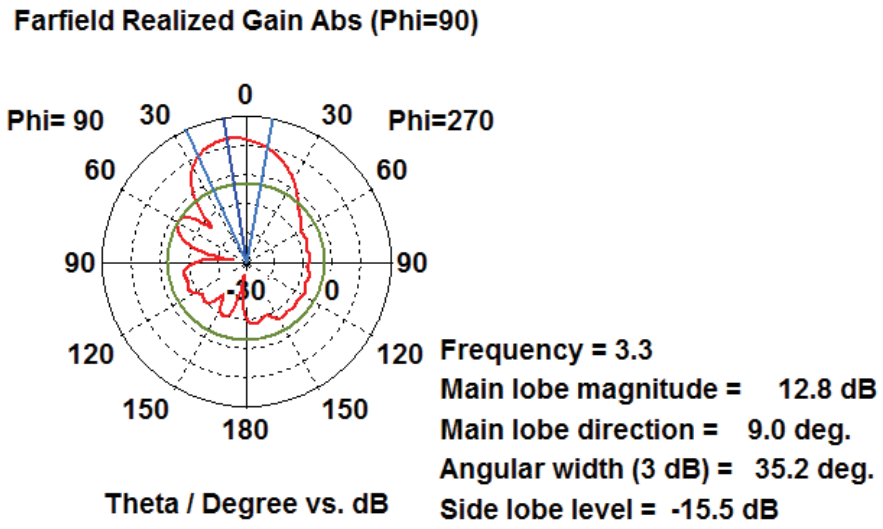

Fig. 6.10 : Bevel-cut simulated gain patterns using CST at ϕ=90°.

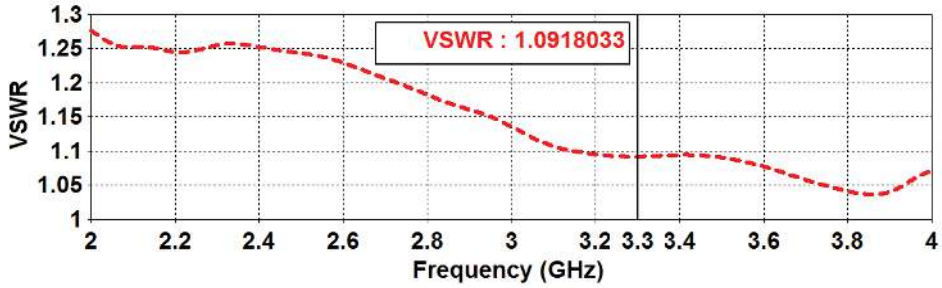

Fig. 6.11 : VSWR plot computed using CST studio.

6.5. Development of S-band MILO

Using the design parameters presented in Chapter 3, engineering drawings for assembly and piece parts drawings are made ,as shown in Fig.6.12 using 'Solid works' modelling software. Further all piece parts of MILO except window is perspex, was fabricated using commercial grade stainless steels material and window is made up of perspex material. The total length of the conical flange is 125 mm, the diameter right side flange is 531 mm, the diameter of left side flange is 250 mm and each flange thickness is 15 mm. A bulk piece of SST was chosen and in which all conical portion with desired dimensions were machined using PROTECH CNC lathe and two flanges

are made using HMT lathe machine and thereafter both flanges are TIG (Tungsten Inert Gas) welded together with conical portion to get vacuum tight joint. The required shape and size of the conical flange were machined using tungsten carbide turning tool by holding on a three jaw chuck. The whole conical structure was machined using specially made tungsten carbide tool.

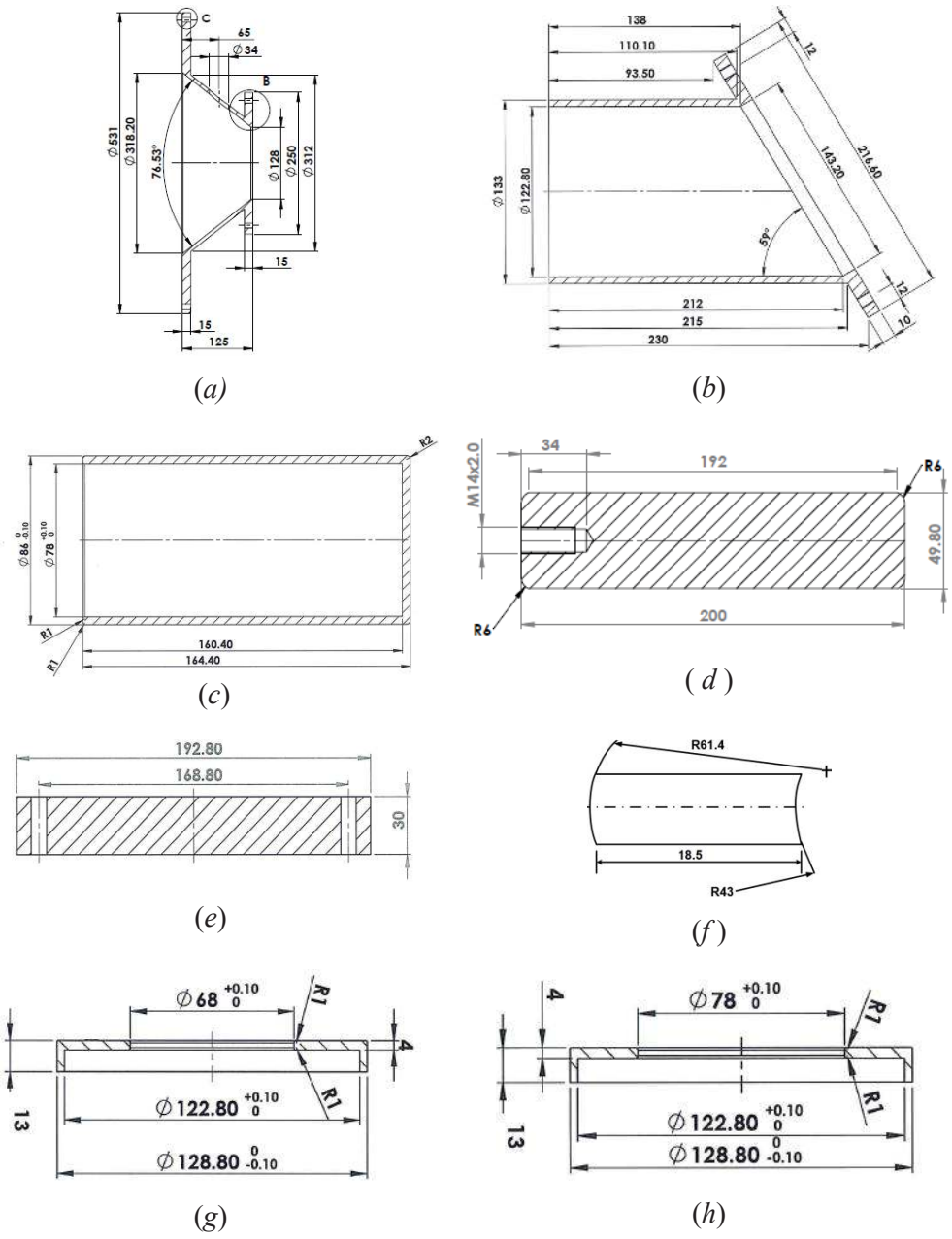

Fig. 6.12 : Piece parts drawings of MILO *(a)* Conical Flange *(b)* Vlasov antenna *(c)* Beam dump *(d)* Cathode (*e*) Window (*f*) Stub (*g*) Choke vane (*h*) SWS vane .

Fig. 6.13: Fabricated piece parts of MILO (*a*) Conical Flange (*b*) Vanes support (*c*) Cathode pasted with velvet (d) Window (*e*) Vanes (*f*) Bell jar (*g*) Vlasov antenna (*h*) Beam dump (*i*) Final assembly of MILO.

After machining all the machined surfaces were polished using metal wool and lapping pastes. The surfaces are to be burr free and needed to be polished to avoid any electric arcing as the parts used for the very high voltage applications. It is desirable to achieve a Roughness surface of Ra 10micrometre through polishing process. It is important to ensure that all the machined surfaces are free from the cutting / lubricant oils which were used during machining. Similarly, the other parts such as choke vanes, SWS vanes, Vlasov antenna, beam dump, cathode, stubs are fabricated using

PROTECH CNC lathe machine with tolerance of ± 100 micrometre and it is desirable to achieve a Roughness surface of Ra 10 micrometre through polishing process. The window is used as vacuum to air seal interface in MILO and it is fabricated with perspex material by using CNC milling machine. Hence, all the piece parts were vapour-degreased using trichloro-ethylene in order to remove oil used while machining the piece parts. Then all the piece parts were inspected for dimensional accuracy and the surface finish. After inspecting the parts of MILO, they have been assembled for electrical testing as shown in Fig.6.12 (h). All the fabricated piece parts of MILO are as shown in Fig.6.13.

6.6. Testing and characterization of S-Band MILO

The S-band MILO developed by MTRDC is tested with available pulse power supply (PPS) at MTRDC, Bangalore as shown in Fig.6.14. This PSS is Marx generator based and it works at the pulse voltage of 600kV and current of 60kA with pulsewidth of 130ns .

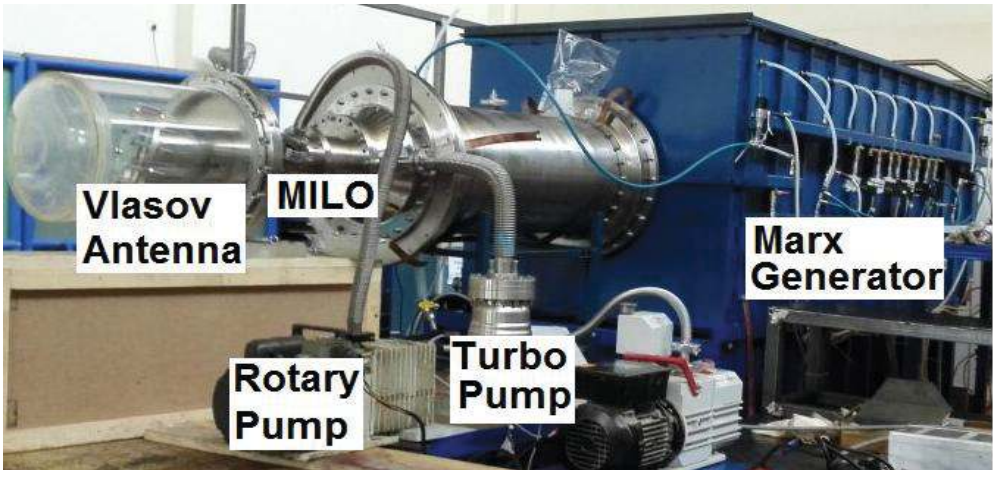

Fig. 6.14 : Experimental set up of MILO at MTRDC.

The experimental set-up comprises high voltage and high current Marx generator, peaking capacitor, S-band MILO device and Vlasov antenna. The primary

supply delivers 440V, 50Hz AC and it is converted into DC voltages by the rectifiers. The DC power supply charges the number of capacitors in parallel between 18-20kV DC and discharges them in series. The Marx generator converts low DC voltage into high impulse voltage of 600kV and applied to peaking capacitor which delivers 600kV with the compressed pulsewidth of 130ns. The transformer oil and glycerine are used as a dielectric inside the Marx generator and peaking capacitor, respectively. The output of peaking capacitor is connected to the S-band MILO where high vacuum around 10^{-5}-10^{-6} Torr is created using the turbo pump (having the pumping capacity of 500 ltrs/sec) backed by the rotary pump. Rough vacuum about 10^{-2} -10^{-3} Torr is created by rotary pump around the mouth of Vlasov antenna for the prevention electrical breakdown due to high RF during testing. The output voltage of peaking capacitor is - 600kV in single shot mode with rise time less than 10ns is applied to MILO where the cathode pasted with velvet cloth using metallic glue emits electrons due to explosive emission phenomena. Initially the charging current is established where all electrons reach from cathode to the anode through beam dump. Once charging current is equal to the critical current, a magnetic insulation condition is established in the RF interaction structure and sustains the EM fields present in the interaction. Then the electrons tend to move perpendicular to E and B-forces along equipotential surfaces**.** When the radial electric field (E_r) and dc electric field (E_o) are in the same direction, electrons are getting accelerated. The electrons are decelerated when both E_r and E_o are in opposite direction. Therefore, electrons bunching take place in the process of acceleration and deceleration. Once magnetic cut-off reached, transient state allows establishment of RF wave in the slow-wave structure. When synchronization of RF phase velocity and electron drift velocity occurs, energy exchange takes place**.** As RF field increases in periodic resonator, spokes are formed due to Diocotron instability through E_r component of RF

wave. Potential energy is ultimately transfered from electron beam to RF wave due to axial electric field (E_z) component of RF wave. The escape electrons coming out of cathode interacts with fundamental mode of the RF structure and generates RF power.

Fig. 6.15 : Measured voltage and current Waveform of MILO

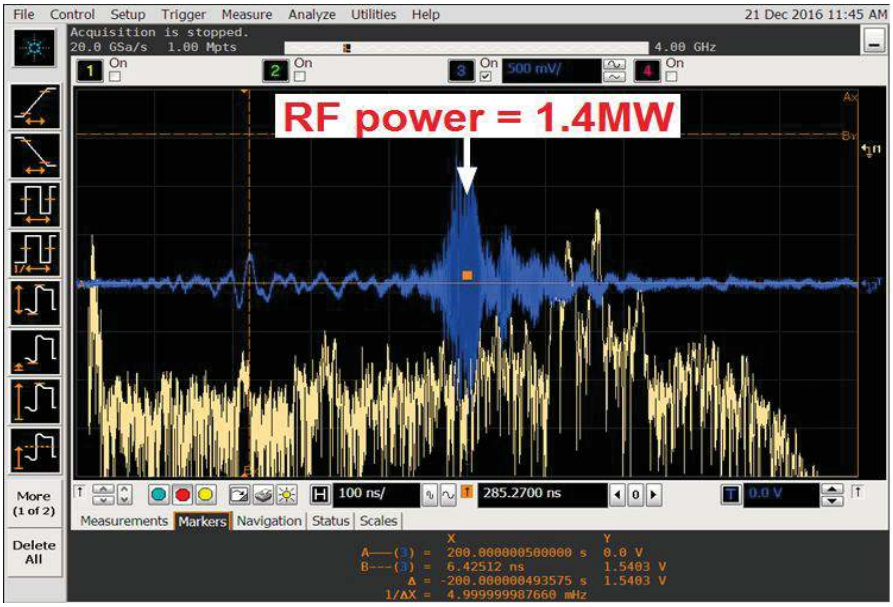

Fig. 6.16 : RF power spectrum of MILO

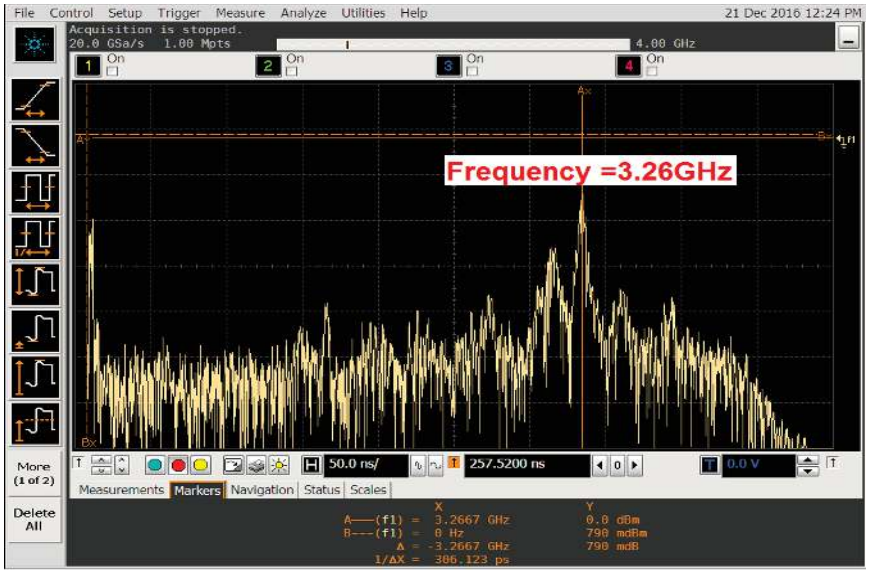

Fig. 6.17 : RF signal frequency spectrum of MILO

The bevel-cut Vlasov antenna is used as the mode convertor as well as an antenna and it is connected in series with MILO device and it is placed inside the anechoic chamber where RF power coming out of antenna gets absorbed without any reflection. The voltage divider has been mounted on the top of peaking capacitor for measuring the voltage delivered to the MILO device as shown in Fig.6.15 (marked in yellow colour). The shielded Rogowski coil is placed at the entrance of MILO for measuring the total anode current of 48.4kA as shown in Fig. 6.15 (marked in green colour). The D-dot sensor is positioned at far field ($2D^2/\lambda$ where D is maximum linear dimension of antenna and λ is free space wavelength) to diagnose the radiated power. Here, radiated far field measurement method is used for RF power diagnostics. Using D-dot sensor, RF output power of 1.4MW as shown in Fig.6.16 at 3.26GHz. Fast Fourier Transform of RF power spectrum as shown in Fig. 6.16 gives the operating frequency of MILO as shown in Fig. 6.17 which is confirmed with design frequency of 3.3GHz.

Reasons for MILO Not-Delivering Giga-Watts of RF Power During Testing:

(a) By using the proper diagnostic instruments in the direction of propagation of microwaves like receiving horn antenna or by using in-guide measurements. Because Vlasov antenna radiates around 34° with respect to the axis of MILO due to conversion of mode from TM_{01} to TE_{11} mode.

(*b*) The melting of velvet cloth pasted on the cathode at three places due to poor vacuum or severe arcing between cathode and SWS vanes, the electrical breakdown inside the MILO due to degassing and RF breakdown due to high RF field near the mouth of an antenna which are all can be prevented by maintaining high vacuum around 10^{-6} -10^{-7} Torr inside the MILO device and rough vacuum better than 10^{-3} Torr around antenna.

(*c*) Window made of Alumina has to be used in place of perspex material because the high RF field delivered by MILO near the mouth of the antenna, RF breakdown occurs due to perspex material having low dielectric strength of $\varepsilon_r = 2.1$ comparing with alumina of $\varepsilon_r = 9.5$.

(*d*) The asymmetric emission of electrons from cathode may be occurring inside the MILO device because the cathode may be offset with respect to the axis of MILO due to cantilever force. This cathode will be corrected by the fitment of cathode with peaking capacitor with proper jigs and fixturing.

(*e*) The gap of extractor cavity between the beam dump and collector may be less and the gap can be adjusted by slightly moving the beam dump in backward direction.

(*f*) The self-magnetic insulation between the cathode and anode is less and it can be checked by measuring the beam dump current and total anode current separately.

6.7. Conclusion

In this chapter, for understanding the concept of self-magnetic insulation between the cathode and anode, MITL has been designed using analytical equations and carried out the numerical simulation using 3D PIC electromagnetic code because MILO works based on the concept of MITL. Based on the design of MITL, the engineering drawings have been made , and the piece parts of MITL have been fabricated with SST material and experiment is completed using pulse power supply (KALI-200) at MTRDC. The concept of self-magnetic insulation due to the generation of azimuthal self-magnetic field in MITL as per the design and simulation is validated by the experiment. Detailed pulse power diagnostics inside the MILO structure and RF power diagnostics at far filed have been explained. Based on the design and simulation presented in chapter 3, the piece parts and final assembly drawings of S-band MILO device are made using solid works modelling software and the piece parts are fabricated using CNC lathe and milling machine with high precision and accuracy. To radiate the RF power from MILO in TE_{11} mode, Vlasov antenna as mode convertor with window has been designed and simulated in CST studio. The piece parts of Vlasov antenna and window are fabricated using SST and perspex material respectively. The S-band MILO device with Vlasov antenna are integrated with high Voltage and high current Marx generator at MTRDC and tested at the beam voltage of 485kV and current of 48.4kA in a single shot mode. The RF output power of 1.4MW has been obtained at the fundamental mode frequency of 3.26GHz which closely matches with the design as discussed in chapter 3. The reasons for not getting gigawatts of RF power as per the design and simulation is enumerated in section 6.6.